Electronic Supplementary information

1. Characterisation Methods:

The physisorption analyses were carried out by degassing the catalysts under N_2 flow for 2 h at 200 °C. The degassed samples were analyzed in a Micrometrics ASAP 2020. Temperature programmed reduction (TPR) was carried out on the catalyst samples using the Micromeritics 2920 Autochem II Chemisorption Analyser. Prior to the reduction of the sample in TPR, the catalyst was pre-treated by heating under a stream of argon (30 mL/min) at 400 °C for 30 min and then cooled to 80 °C. Thereafter, 15 % butane in Ar was used as a reducing agent at a flow rate of 30 mL/min. Samples were analyzed from room temperature to 600 °C using a ramp rate of 10 °C/min. The amount of reductant consumed was measured using a thermal conductivity detector.

Metal dispersion on the surface of the catalyst was measured using O_2-Pulse chemisorption also performed by an AutoChem II 2920 station from Micromeritics as explained in [1]. The samples (300 mg), placed in a U-shaped quartz reactor with an inner diameter of 0.5 cm, were pre-treated under 5% H_2 in Ar a temperature of 500 °C for 2 h. Then, the catalyst was cooled down to 80 °C under a He flows of 50 mL/min and maintain at this temperature for 3 h before further heating to the desired temperature for chemisorptions in order to clean the catalyst surface and to avoid the presence of residual adsorbed hydrogen. O_2-Pulse chemisorption was performed at a temperature of 450 °C. The volume of the injection loop was 0.5 cm^3. The carrier gas was Ar in the case of O_2 pulses (5% O_2 in Ar,) and pulses of O_2 were injected into the catalytic reactor corresponding to 0.5 μmol of O_2 The O_2 consumption was measured with the same TCD used for TPR equipped with a water trap. Pulses injection, sample temperature, and TCD signals were controlled and monitored by a computer equipped with the software Micromeritics AutoChemII. TCD data were analyzed using the Origin software.

Acidity and basicity of the catalyst was measured by NH_3 and CO_2 desorption methods using Micromeritics 2920 Autochem II Chemisorption Analyser. The catalyst was pre-treated at 350 °C under the stream of helium for 60 min in order to remove the physisorbed gases on the surface of the catalysts. The temperature was then decreased to 80 °C. Appropriate gas was passed over the catalyst (9.8 % NH_3 in He / 10 % CO_2 in He) and at a flow rate of 30 mL/min for 60 min. The excess gas was removed by purging with helium for 30 min. The temperature was then raised gradually to 600 °C by ramping at 10 °C/min under the flow of helium and desorption data of NH_3 or CO_2 was recorded. Particle size, morphology and elemental mapping,

performed by EDXS analysis, were further investigated using Cs-corrected scanning transmission electron microscope (TEM) (JEOL, JEM-ARM200CF), equipped with JEOL Centurio 100 mm^2 EDXS system.

The X-ray photoelectron spectroscopy (XPS or ESCA) analyses were carried out on the PHI-TFA XPS spectrometer produced by Physical Electronics Inc. using X-ray radiation from monochromatic Al source. The analyzed area was 0.4 mm in diameter and the analyzed depth was about 3 - 5 nm. The survey wide-energy spectra were taken with pass energy of analyzer of 187 eV and the high-energy resolution spectra were taken with pass energy of 29 eV. Spectra were aligned by setting the C 1s peak at 284.8 eV, characteristic for C-C/C-H bonds. The accuracy of binding energies was about ±0.3 eV.

The main catalyzed products were analyzed by using Perkin Elmer Clarus 400 FID and TCD gas chromotographs. In the GC, the flame ionization detector (FID) connected to a SGE BP-PONA capillary column (0.25 mm ID and 50 m length) was used to analyze the organic products at oven temperatures ramping between 40 and 200 °C. The thermal conductivity detector (TCD) with a SUPELCO Carboxen (0.53 mm ID and 30 m length) column was used to analyze the carbon oxides. The signals of GC were calibrated using the mixtures with different moles of products that are in order to determine the moles of the gases in the outflow.A Perkin Elmer Clarus 500 GC–MS was used to identify unknown products from the reaction stream. The calculated carbon balance was between 97 and 100%. All data points were obtained in duplicate with an error of ±2%.

The rate constant “k” was obtained using the integrated rate law (An introduction to chemical kinetics by Claire Vallance, Morgan & Claypool Publishers, 2017), by using the moles of butane present in inlet and outlet gases in a unit time (3 h) at a particular temperature. The rates were determined at a particular temperature in the range of 300 °C and 500 °C. The natural log of the rate constant (-lnk) was plotted versus the inverse of the temperature (1/T) (Temperature varied from 300 °C and 500 °C) resulted in a straight line with a slope of (-Ea/R), which used to determine the apparent activation energy.

X-ray powder diffraction patterns for the catalysts were collected at room temperature on a laboratory PANalytical X'Pert PRO diffractometer using $CuK\alpha_1$ radiation (1.54060 Å). The samples were loaded into a flat disc like sample holder. The XRPD data were collected in the 2θ range from 10 to 90º 2Θ in steps of 0.017˚ 2Θ and 1012 s per step and using a fully opened

X'Celerator detector. The qualitative and quantitative powder analysis with Rietveld refinement of the collected XRPD patterns was performed using the X'Pert High Score Plus Suite [2] and Topas-Academic v.4 software package [3]. Final Rietveld refinement converged with acceptable agreement factors of R_{wp} = 9.8% for SCR, R_{wp} = 13.2%, for SCR-RED-600, R_{wp} = 13.4% for SCR-300-NO and R_{wp} = 13.9% for SCR-RED-500-NO.

In the Rietveld refinement the identified phases in each sample were taken into account. The diffraction peaks profiles were approximated using FP or Double-Voigt approach. The refined parameters in the final cycle were 8 background polynomial parameters, zero shift, absorption correction, and for each phase lattice parameters, scale factors, and crystallite size.

Crystal data and final refinement parameters for SCR sample:

Phase name 1	TiO2-anatase
Unit cell edges (Å)	a=3,785(1), c=9.510(3)
Phase wt%	95,2(3)
Phase name 2	TiO2-rutile
Unit cell edges (Å)	a=7,087(3), c=6.270(4)
Phase wt%	1,5(3)
Phase name 3	WO_3
Unit cell edges (Å)	a=7,31(1), c=7,53(1), c=7,74(1)
Phase wt%	1,2(1)
Phase name 4	WVO_4
Unit cell edges (Å)	a=4,592(2), c=2,960(3)
Phase wt%	2.1(1)
R_{wp}(%)	9.82
Profile function	Fundamental parms., Double-Voigt approach
Background function	Polynomial Chebychev, order 8

Crystal data and final refinement parameters for SCR-RED-600 sample:

Phase name 1	TiO2-anatase
Unit cell edges (Å)	a=3,7855(4), c=9.509(1)
Phase wt%	98,7(1)
Phase name 2	VO
Unit cell edges (Å)	a=4,0534(4)
Phase wt%	0,98(8)
Phase name 3	WO_3
Unit cell edges (Å)	a=7,38(4), c=7,55(4), c=7,75(4)
Phase wt%	0,27(6)
R_{wp}(%)	13.24
Profile function	Fundamental parms., Double-Voigt approach
Background function	Polynomial Chebychev, order 8

Crystal data and final refinement parameters for SCR-300-NO sample:

Phase name 1	TiO2-anatase
Unit cell edges (Å)	a=3,7818(4), c=9.499(1)
Phase wt%	97,0(2)
Phase name 2	$V_{2-x}Ti_xO_3$
Unit cell edges (Å)	a=5,034(1), c=13,738(5)
Phase wt%	2,2(2)
Phase name 3	WO_3
Unit cell edges (Å)	a=7,4324), c=7,52(2), c=7,60(2)
Phase wt%	0,72(7)

R_{wp}(%)	13.39
Profile function	Fundamental parms., Double-Voigt approach
Background function	Polynomial Chebychev, order 8

Crystal data and final refinement parameters for SCR-RED-500-NO sample:

Phase name 1	TiO2-anatase
Unit cell edges (Å)	a=3,7848(5), c=9.505(1)
Phase wt%	98,7(1)
Phase name 2	VO
Unit cell edges (Å)	a=4,0527(4)
Phase wt%	0,8(1)
Phase name 3	WO_3
Unit cell edges (Å)	a=7,45(3), c=7,55(3), c=7,70(3)
Phase wt%	0,49(6)
R_{wp}(%)	13.92
Profile function	Fundamental parms., Double-Voigt approach
Background function	Polynomial Chebychev, order 8

2. Mass and Heat Transfer Calculations for n-butane oxidation over Ni-Mo/Al_2O_3 catalyst

Mears Criterion for External Diffusion (Fogler, p841; Mears, 1971)

n-butane activation over oxygen:

If $\frac{-r_A'\rho_b Rn}{k_c C_{Ab}} < 0.15$, then external mass transfer effects can be neglected.

$-r_A'$ = reaction rate, kmol/kg-cat · s = 6.53 x 10^{-4} kmol-C_3/kg-cat . s

n = reaction order = 2

R = catalyst particle radius, m=2 x 10^{-4} m

ρ_b = bulk density of catalyst bed, kg/m^3

=(1-ϕ) (ϕ= porosity or void fraction of packed bed)= 1035 kg/m^3

ρ_c = solid catalyst density, kg/m^3= 1.42 m/s

C_{Ab} = bulk gas concentration of A, kmol/m^3 = 0.0075 kmol/m^3

k_c = mass transfer coefficient, m/s = 1.25 m/s

$\frac{-r_A'\rho_b Rn}{k_c C_{Ab}}$ **= 8.32 x 10^{-3} <0.15 {Mears for External Diffusion}**

Similarly, for NO = 1.22 x 10^{-3}

3. Weisz-Prater Criterion for Internal Diffusion (Fogler, p839)

If $C_{WP} = \frac{-r'_{A(obs)}\rho_c R^2}{D_e C_{As}} < 1$, then internal mass transfer effects can be neglected.

-r'$_{A(obs)}$ = observed reaction rate, kmol/kg-cat · s = 6.53 x 10^{-4} kmol-C_3/kg-cat . s

R = catalyst particle radius, m=2 x 10^{-4} m

ρ_c = solid catalyst density, kg/m^3 = 1420 kg/m^3

D_e = effective gas-phase diffusivity, m^2/s **[Fogler, p815]**

$= \frac{D_{AB}\phi_p\sigma_c}{\tau}$ where

D_{AB} = gas-phase diffusivity m^2/s; ϕ_p = pellet porosity; σ_c =constriction factor; τ =tortuosity.

C_{As} = gas concentration of A at the catalyst surface, kmol-A/m^3 = 0.0038 kmol-C3/m^3

$$C_{WP} = \frac{-r'_{A(obs)}\,\rho_c R^2}{D_e C_{As}} = \textbf{4.0 x } \mathbf{10^{-3} < 1}$$ **{Weisz-Prater Criterion for Internal Diffusion}**

Similarly, for NO = 2.12 x 10^{-3}

4. Mears Criterion for Combined Interphase and Intraparticle Heat and Mass Transport (Mears, 1971)

$$\frac{-r'_A R^2}{C_{Ab} D_e} < \frac{1+0.33\gamma\chi}{\left|n-\gamma_b\beta_b\right|\left(1+0.33n\omega\right)}$$

$$\gamma = \frac{E}{R_g T_s};\ \gamma_b = \frac{E}{R_g T_b};\ \beta_b = \frac{\left(-\Delta H_r\right) D_e C_{Ab}}{\lambda T_b};\ \ \chi = \frac{\left(-\Delta H_r\right) - r'_A R}{h_t T_b};\ \ \omega = \frac{-r'_A R}{k_c C_{Ab}}$$

γ = Arrhenius number; β_b = heat generation function;

λ = catalyst thermal conductivity, W/m.K;

χ = Damköhler number for interphase heat transport

ω = Damköhler number for interphase mass transport

$\frac{-r'_A R^2}{C_{Ab} D_e}$ **= 2.82 x10^{-4} < 3{Mears Criterion for Interphase and Intraparticle Heat and Mass Transport }**

Similarly, for NO = 1.24 x 10^{-4}

Table S1: The effect of metal oxide, support and promoter on the *n*-butane oxidative activation

Catalyst	***n*-butane conversion (mol %)**	**Oxidant**	**Temperature**	**TOF (s^{-1})**	**Reference**
7 % V_2O_5/SiO_2	1.2	Air	230	0.4 x 10^{-5}	[4, 5]
17.5 % V_2O_5/Al_2O_3	7.2	Air	230	0.9 x 10^{-5}	[4, 5]
6 % V_2O_5/Nb_2O_5	17.3	Air	230	3.6 x 10^{-5}	[4, 5]
4 % V_2O_5/ZrO_2	16.0	Air	230	4.5 x 10^{-5}	[4]
3 % V_2O_5/CeO_2	10.6	Air	230	6.3 x 10^{-5}	[4]
5 % V_2O_5/TiO_2	27.8	Air	230	19.6 x 10^{-5}	[4]
1 % V_2O_5/ 5 % P_2O_5/TiO_2	12.1	Air	230	27.0 x 10^{-5}	[4]
6 % WO_3/ 1 % V_2O_5/TiO_2	23.6	Air	230	34.1 x 10^{-5}	[4]
γ-Bi_2MoO_6	30.2	Air+steam	420	43.6 x 10^{-4}	[6]
β-$Bi_2Mo_2O_9$	39.8	Air+steam	320	57.8 x 10^{-4}	[6]
$BiMoZr_x$ oxide	42.3	Air	440	6.11 x 10^{-4}	[7]
$BiMoFe_x$ oxide	68.6	Air	420	9.23 x 10^{-4}	[8]
$ZrFe_{2-x}Al_xO_4$	55.1	Air	420	7.96 x 10^{-4}	[9]
$ZnFe_2O_4$	41.3	Air	420	5.97 x 10^{-4}	[6, 10]
TiP_2O_7-M1	24.0	CO_2	530	3.47 x 10^{-4}	[11]
TiP_2O_7-M2	22.3	CO_2	530	3.22 x 10^{-4}	[11]
1.2 % Cr 2.8 % V/MCM-41	10.2	CO_2	550	1.47 x 10^{-4}	[12]
1.2 % Cr 2.8 % V/ZSM-5	8.3	CO_2	550	1.20 x 10^{-4}	[12]
1.2 % Cr 2.8 % V/ MCM-22	7.2	CO_2	550	1.04 x 10^{-4}	[12]
1.2 % Cr 2.8 % V/ZSM-5(Mesoporus)	6.1	CO_2	550	8.81 x 10^{-5}	[12]

Table S2: Influence of oxidant (O_2) in the feed over V_2O_5-WO_3/TiO_2 catalyst at temperatures of 350 °C. (Feed Composition: 15 % butane, O_2 to butane ratio of 2, GHSV = 4600 h^{-1})

Time (min)	Conversion (%)	Selectivity (mol %)				Oxidant (O_2) conversion (%)	Carbon balance (%)
		C_4H_6	C_4H_8	Cracked Products	CO_X		
Oxidant (O_2) in the feed							
30	38.2	34.2	13.8	22.3	29.7	96	98
60	37.9	35.1	13.5	22.5	28.9	95	97
90	38.4	34.9	13.7	22.7	28.7	97	99
120	37.5	34.5	13.1	22.4	30.0	96	98
150	38.1	34.3	13.4	22.9	29.4	97	99
Oxidant (O_2) removed from the feed							
180	25.3	44.5	22.1	18.3	15.1	0	95
210	19.4	48.3	24.1	27.6	0	0	94
240	13.5	45.5	25.1	29.4	0	0	95
270	14.1	46.3	24.9	28.8	0	0	96
300	13.9	45.1	25.3	29.6	0	0	96
Oxidant (O_2) restored to the feed							
330	21.8	39.3	22.2	35.3	3.2	99	98
360	32.7	35.6	19.5	35.3	9.6	98	99
390	35.3	35.1	22.5	28.3	14.1	97	98
420	33.2	35.9	21.3	27.2	15.6	98	99
450	34.5	35.5	20.2	26.1	18.2	99	99

Table S3: Influence of oxidant (O_2) in the feed over V_2O_5-WO_3/TiO_2 catalyst at temperatures of 450 °C. (Feed Composition: 15 % butane, O_2 to butane ratio of 2, GHSV = 4600 h^{-1})

Time (min)	Conversion (%)	Selectivity (mol %)				Oxidant (O_2) conversion (%)	Carbon balance (%)
		C_4H_6	C_4H_8	Cracked Products	CO_X		
Oxidant (O_2) in the feed							
30	71.3	45.8	9.8	14.6	29.8	100	97
60	69.5	44.2	10.3	16.2	29.3	100	99
90	70.5	45.5	11.2	14.1	29.2	100	98
120	71.2	44.9	10.5	16.1	28.5	100	98
150	71.1	45.1	10.1	16.5	28.3	100	100
Oxidant (O_2) removed from the feed							
180	52.8	58.3	14.2	27.5	0	0	99
210	45.2	61.2	16.5	22.3	0	0	101
240	44.5	61.5	16.8	21.7	0	0	99
270	45.8	60.3	16.4	23.3	0	0	98
300	44.1	59.5	16.5	24.0	0	0	97
Oxidant (O_2) restored to the feed							
330	49.5	55.2	14.5	6.2	24.1	100	99
360	62.5	48.5	13.2	13.1	25.2	100	101
390	68.2	45.3	13.1	13.3	28.3	100	97
420	68.9	44.5	13.5	14.8	27.2	100	99
450	68.7	44.9	13.8	15.2	26.1	100	98

Table S4: Influence of oxidant (NO) in the feed over V_2O_5-WO_3/TiO_2 catalyst at temperatures of 350 °C. (Feed Composition: 15 % butane, NO to butane ratio of 2, GHSV = 4600 h^{-1})

Time (min)	Conversion (%)	Selectivity (mol %)				Oxidant (NO) conversion (%)	Carbon balance (%)
		C_4H_6	C_4H_8	Cracked Products	CO_X		
Oxidant (NO) in the feed							
30	25.6	57.2	27.2	7.1	8.5	100	99
60	25.9	55.3	25.7	10.3	8.7	100	98
90	25.4	53.7	26.3	11.5	8.5	100	101
120	25.8	54.9	25.9	11.1	8.1	100	99
150	25.9	55.7	26.9	9.1	8.3	100	97
Oxidant (NO) removed from the feed							
180	18.3	56.3	28.4	10.1	5.2	0	98
210	17.2	58.9	26.3	14.8	0	0	95
240	17.5	65.7	27.1	7.2	0	0	96
270	17.8	67.2	28.3	4.5	0	0	95
300	17.9	68.2	27.5	4.3	0	0	96
Oxidant (NO) restored to the feed							
330	19.3	65.3	26.3	2.2	6.2	100	101
360	20.1	64.1	29.2	0.4	6.3	100	100
390	20.5	63.2	23.1	6.8	6.9	100	99
420	21.8	62.5	22.5	7.8	7.2	100	97
450	22.1	64.1	24.3	4.5	7.1	100	99

Table S5: Influence of oxidant (NO) in the feed over V_2O_5-WO_3/TiO_2 catalyst at temperatures of 450 °C. (Feed Composition: 15 % butane, NO to butane ratio of 2, GHSV = 4600 h^{-1})

Time (min)	Conversion (%)	Selectivity (mol %)				Oxidant (NO) conversion (%)	Carbon balance (%)
		C_4H_6	C_4H_8	Cracked Products	CO_X		
Oxidant (NO) in the feed							
30	35.2	67.2	17.2	7.1	8.1	100	98
60	35.9	65.3	15.7	10.3	8.6	100	99
90	35.4	64.7	16.3	10.5	8.3	100	99
120	35.8	65.9	15.9	10.1	8.3	100	98
150	35.9	68.3	16.9	6.5	8.9	100	99
Oxidant (NO) removed from the feed							
180	28.3	56.3	18.4	20.1	0	0	97
210	27.25	58.9	16.3	24.8	0	0	98
240	27.5	65.7	17.1	17.2	0	0	95
270	27.8	67.2	18.3	14.5	0	0	96
300	27.9	68.2	17.5	14.3	0	0	97
Oxidant (NO) restored to the feed							
330	29.3	65.3	16.3	12.2	6.1	100	98
360	30.1	64.1	19.2	10.4	5.5	100	99
390	30.5	63.2	13.1	16.8	5.6	100	101
420	31.8	62.5	12.5	17.8	5.5	100	98
450	32.1	64.1	14.3	14.5	5.3	100	98

3. Kinetics of reduction and oxidation:

The kinetics of reduction and oxidation was calculated using Autochem 2920 Chemisorption analyser. A series of reduction (TPR) and oxidation (TPO) experiments (as explained in Experimental section) were done at different heating rates namely 2 °C/min, 5 °C/min, 7 °C/min, 10 °C/min, 14 °C/min and 20 °C/min. The data are plotted and the slope determined to calculate the rate, activation energy for reduction and oxidation [13].

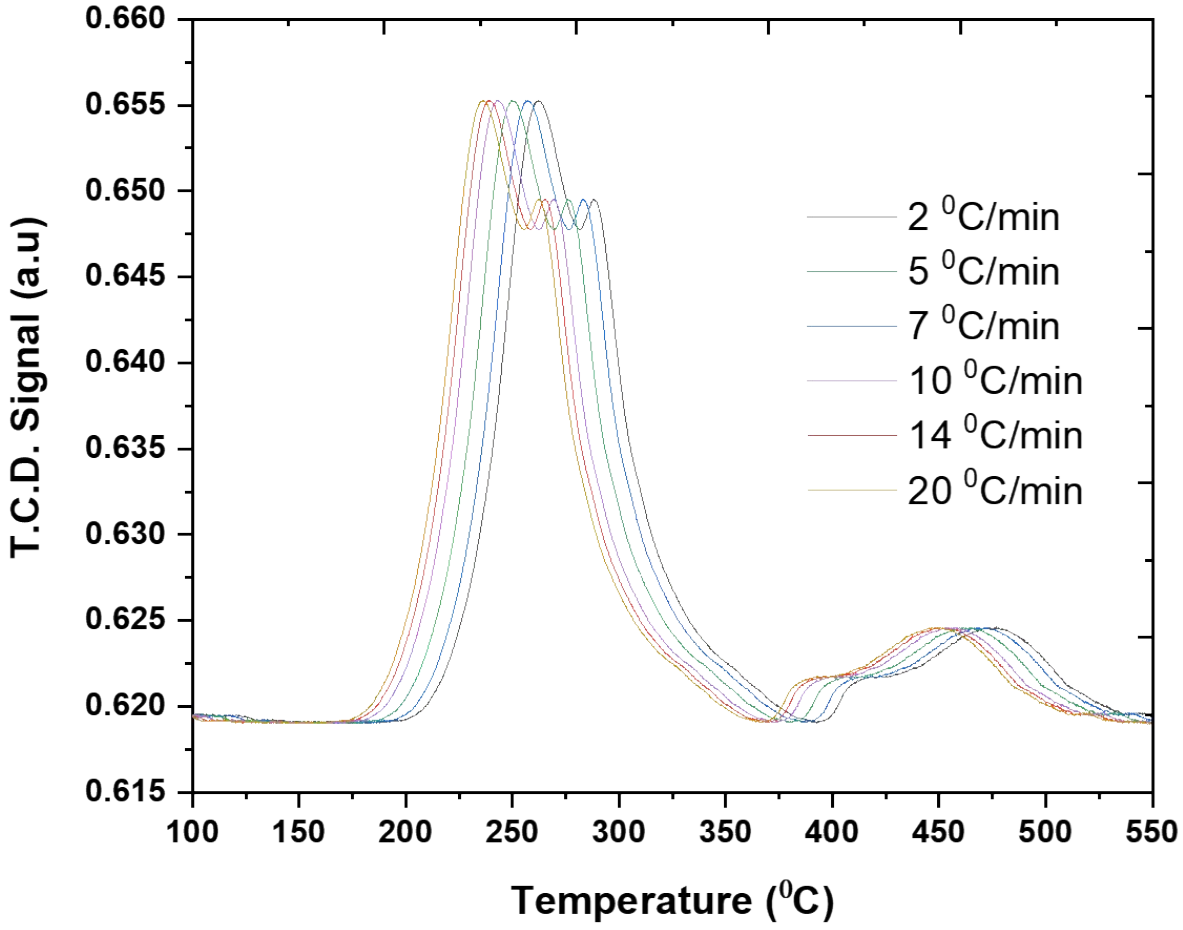

Figure S1: First order kinetics of reduction experiments of V_2O_5- WO_3/TiO_2 catalyst

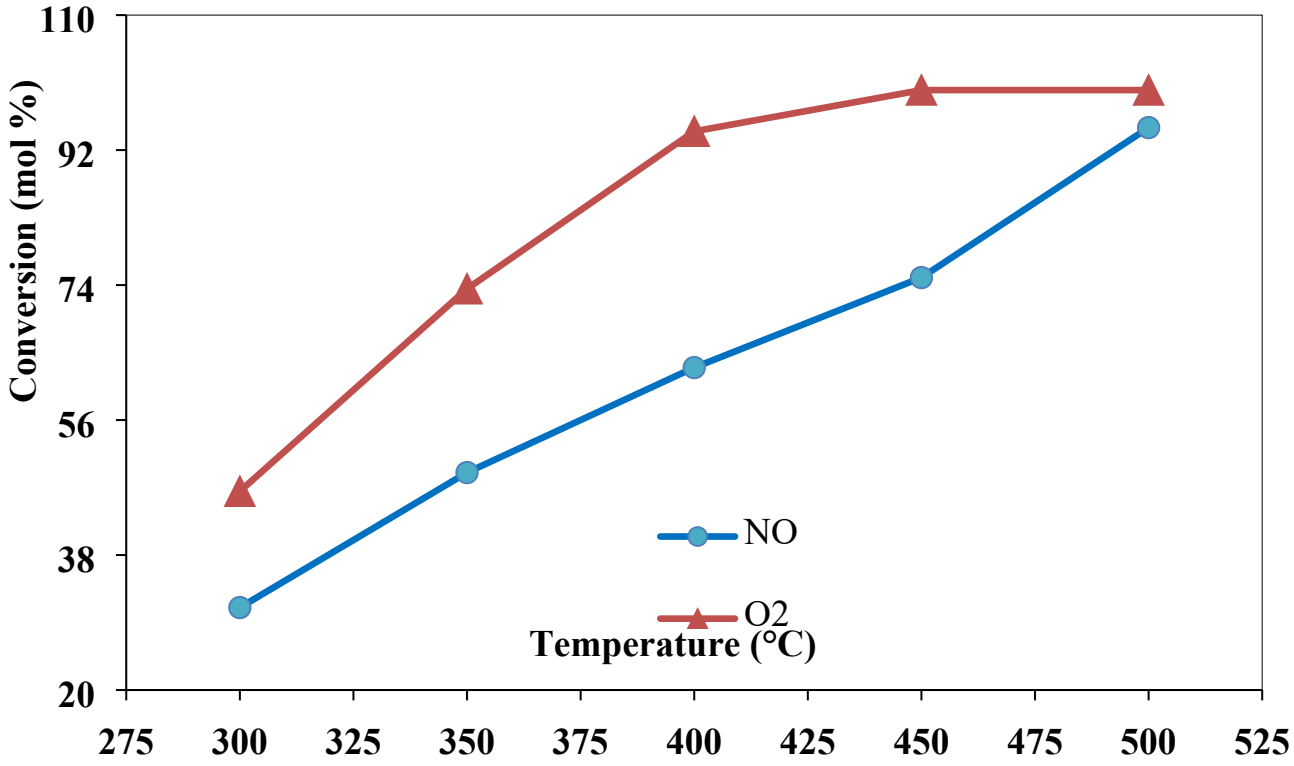

Figure S2: Influence of temperature on the conversion of oxidant (NO and O_2) in oxidative dehydrogenation of butane with the V_2O_5-WO_3/TiO_2 catalyst. Feed Composition: 15 % butane, oxidant to butane ratio of 2, GHSV = 4600 h^{-1}.

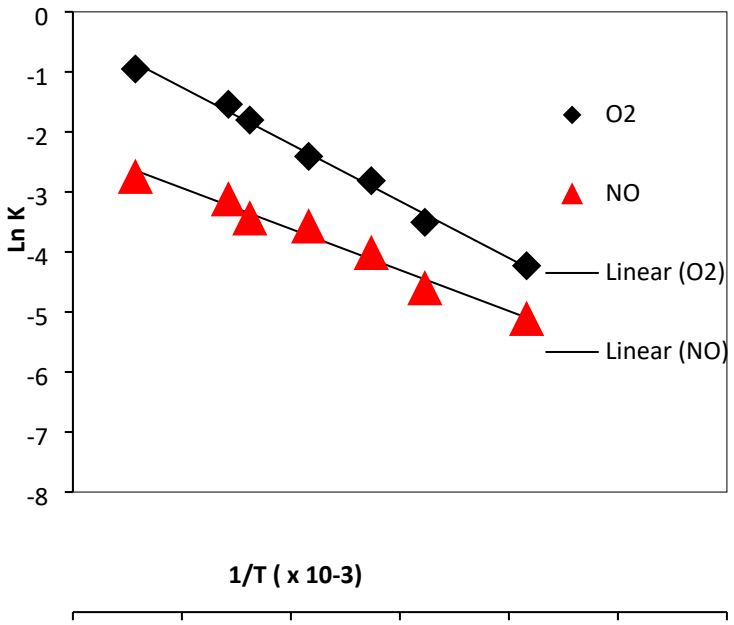

Figure S3: Arrhenius relationship profile of *n*-butane activation over V_2O_5- WO_3/TiO_2 catalyst with O_2 and NO as oxidants

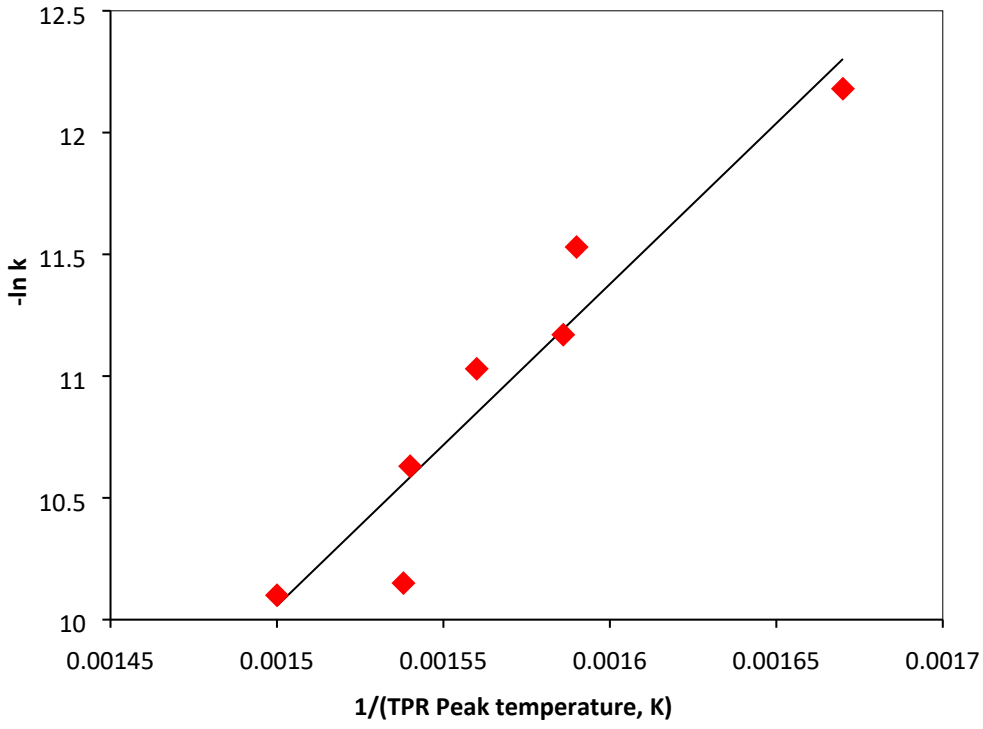

Figure S4: Arrhenius relationship profile of reduction (15 % butane in He) of V_2O_5-WO_3/TiO_2 catalyst

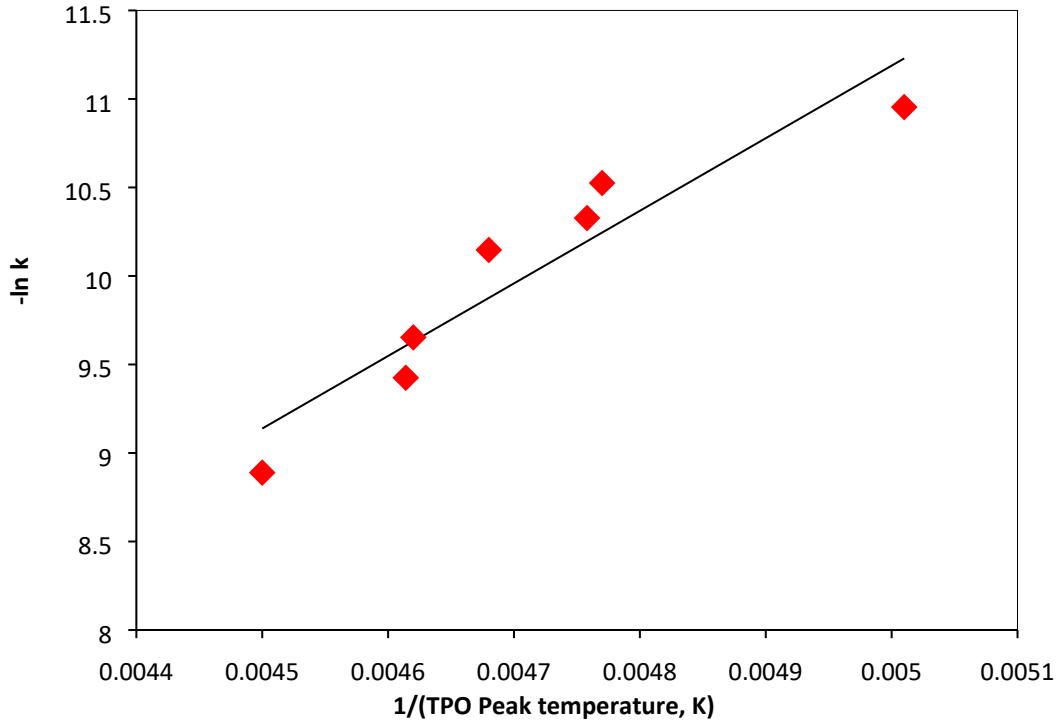

Figure S5: Arrhenius relationship profile of oxidation (with O_2) of V_2O_5- WO_3/TiO_2 catalyst

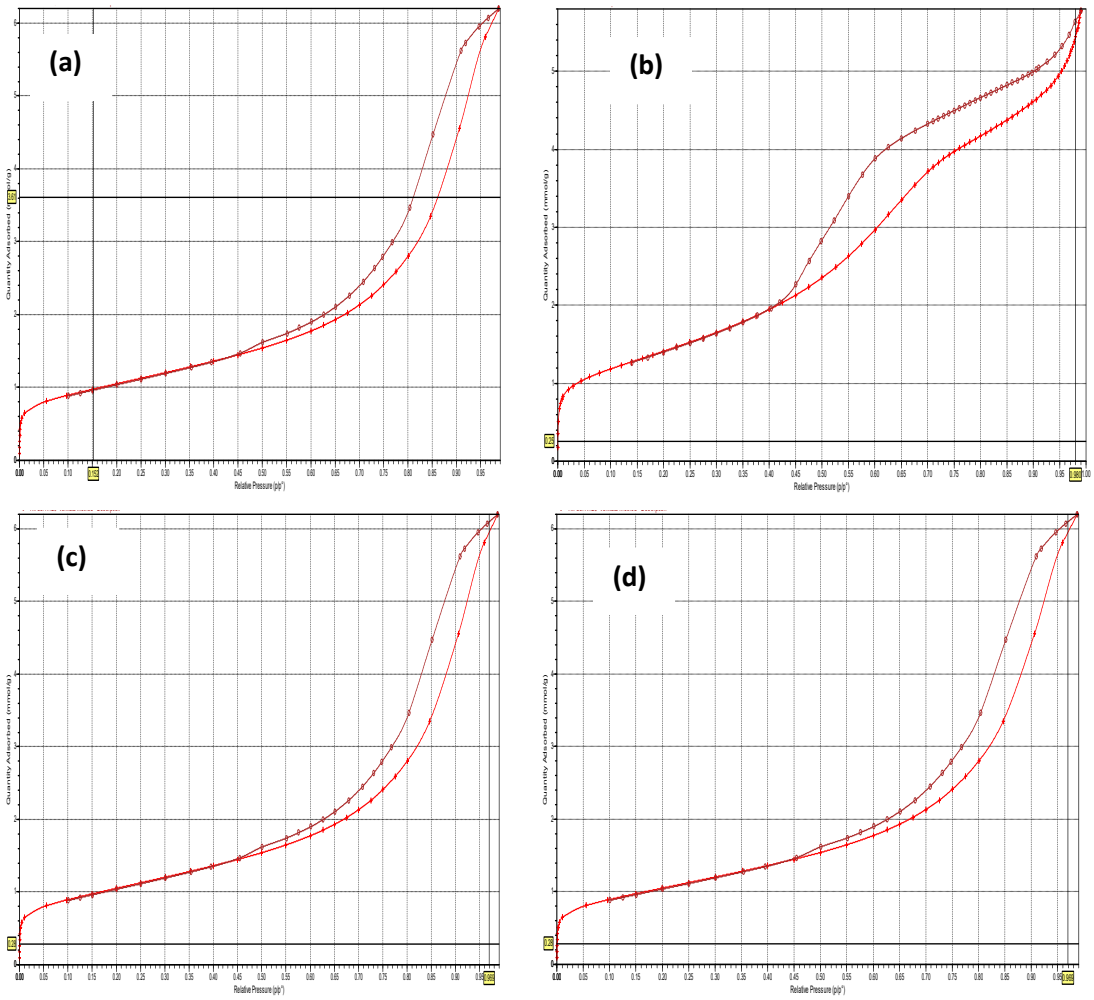

Figure S6: N_2 physisorption analysis of (a) fresh, (b) reduced, (c) re-oxidised (with O_2) at 350 °C and (d) Re-oxidised (with O_2) at 450 °C

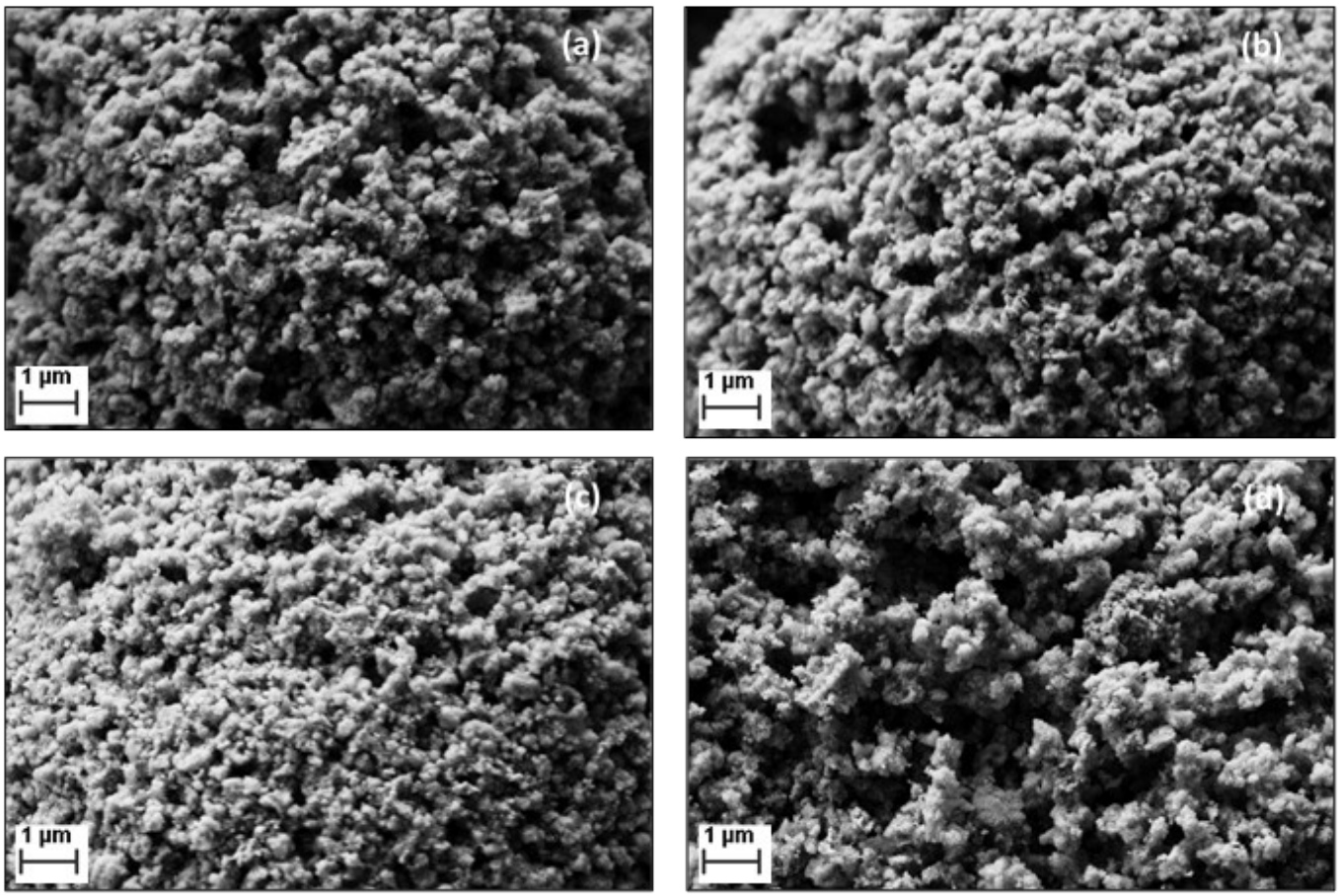

Figure S7: Scanning Electronic Microscopic images of V_2O_5- WO_3/TiO_2 catalyst (a) fresh, (b) reduced, (c) re-oxidised (with O_2) at 350 °C and (d) Re-oxidised (with O_2) at 450 °C

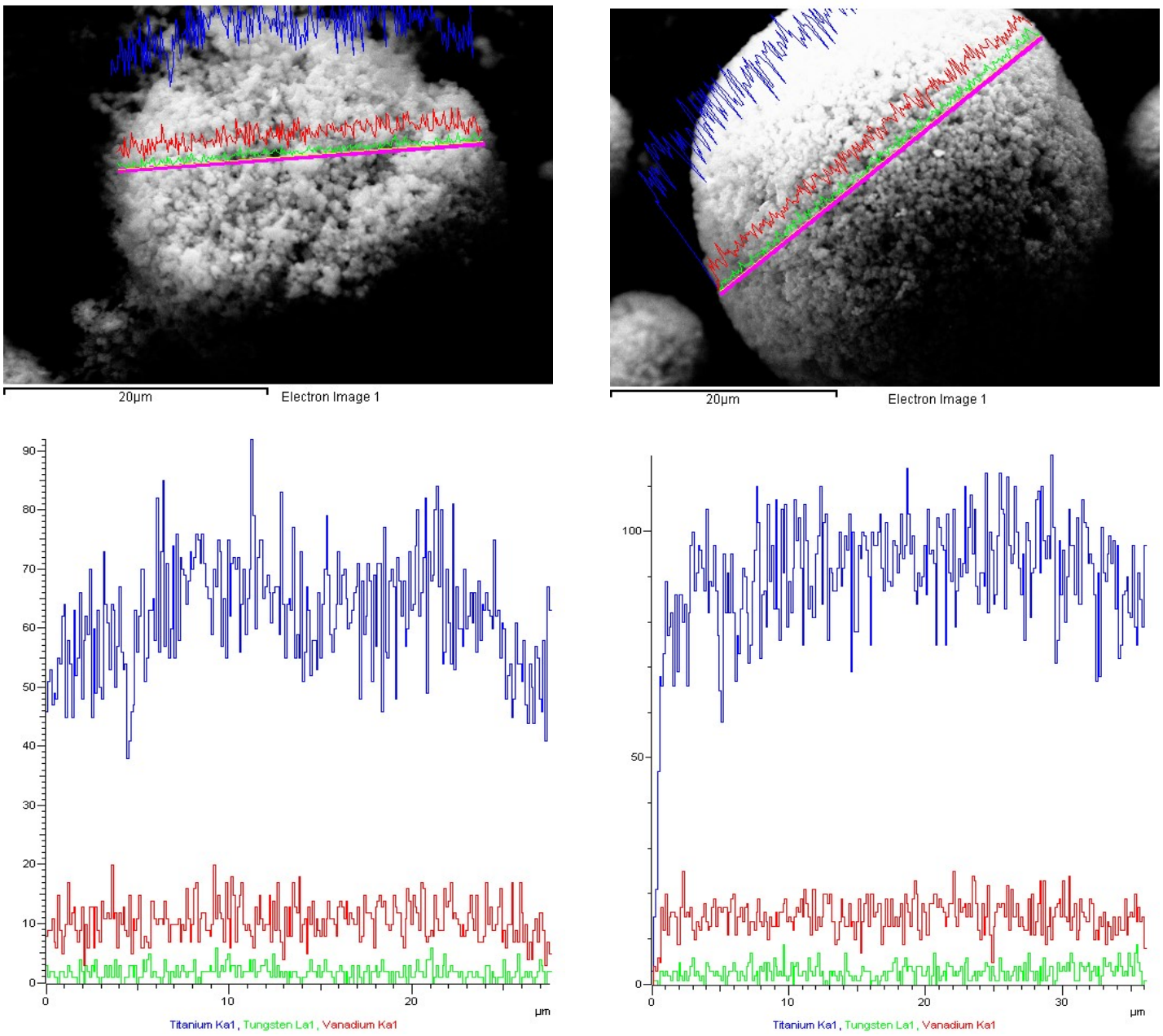

Figure S8: SEM-EDX (Line scanning) analysis of V_2O_5-WO_3/TiO_2 catalyst

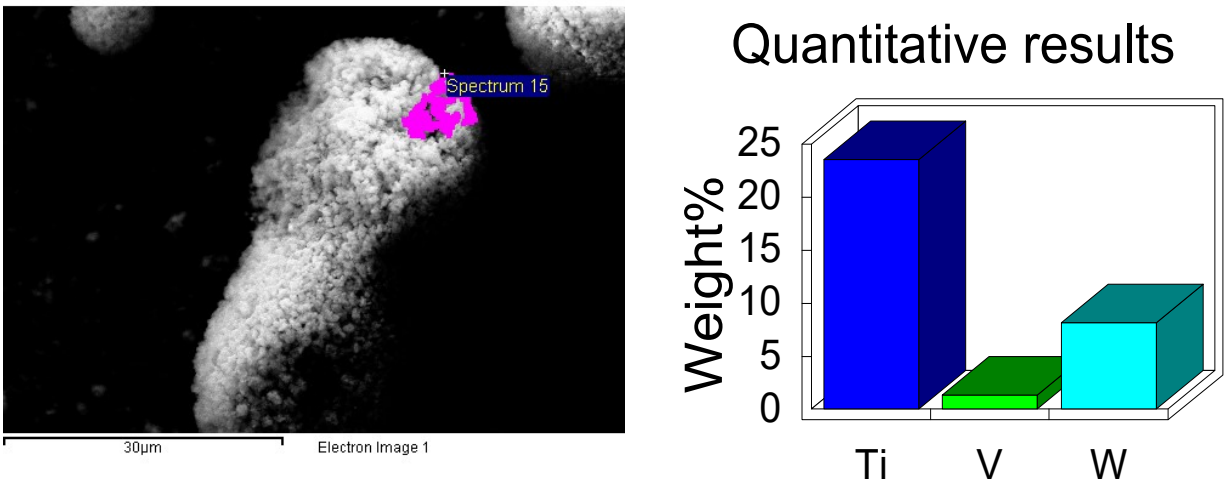

Figure S9: Elemental quantitative analyses of V_2O_5-WO_3/TiO_2 catalyst

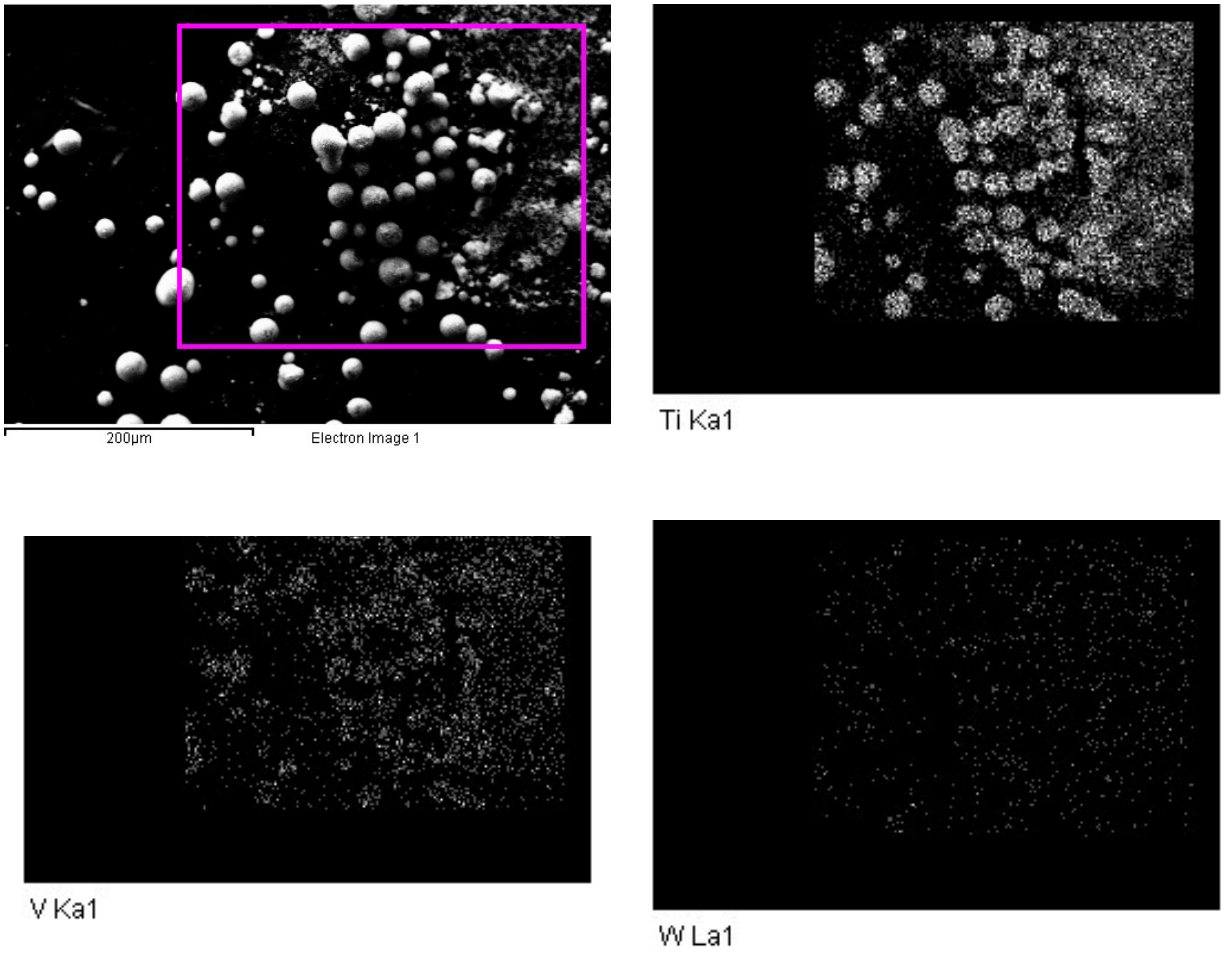

Figure S10: SEM-EDX Elemental mapping of V_2O_5-WO_3/TiO_2 catalyst

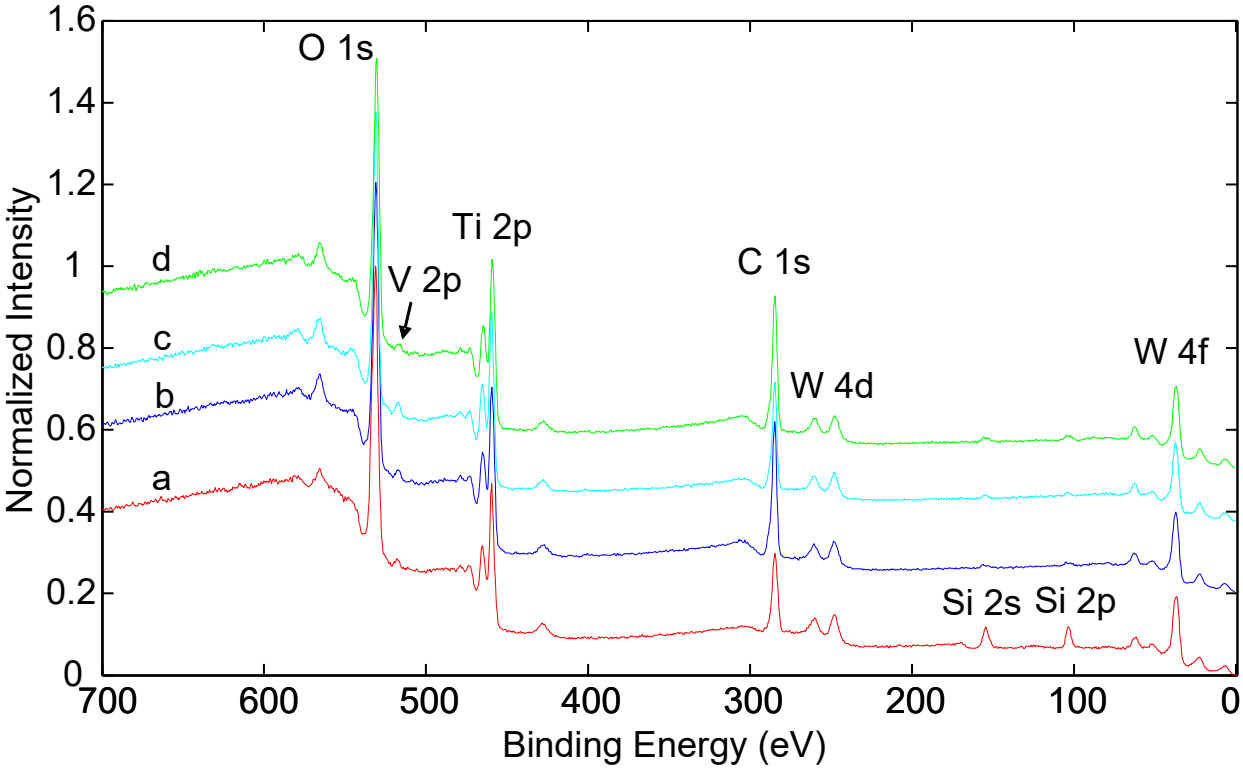

Figure S11 : XPS spectra from (a) pure sample, (b) reduced sample, (c) sample oxidised at 300 °C (with NO) and (d) sample oxidised at 500 °C (with NO).

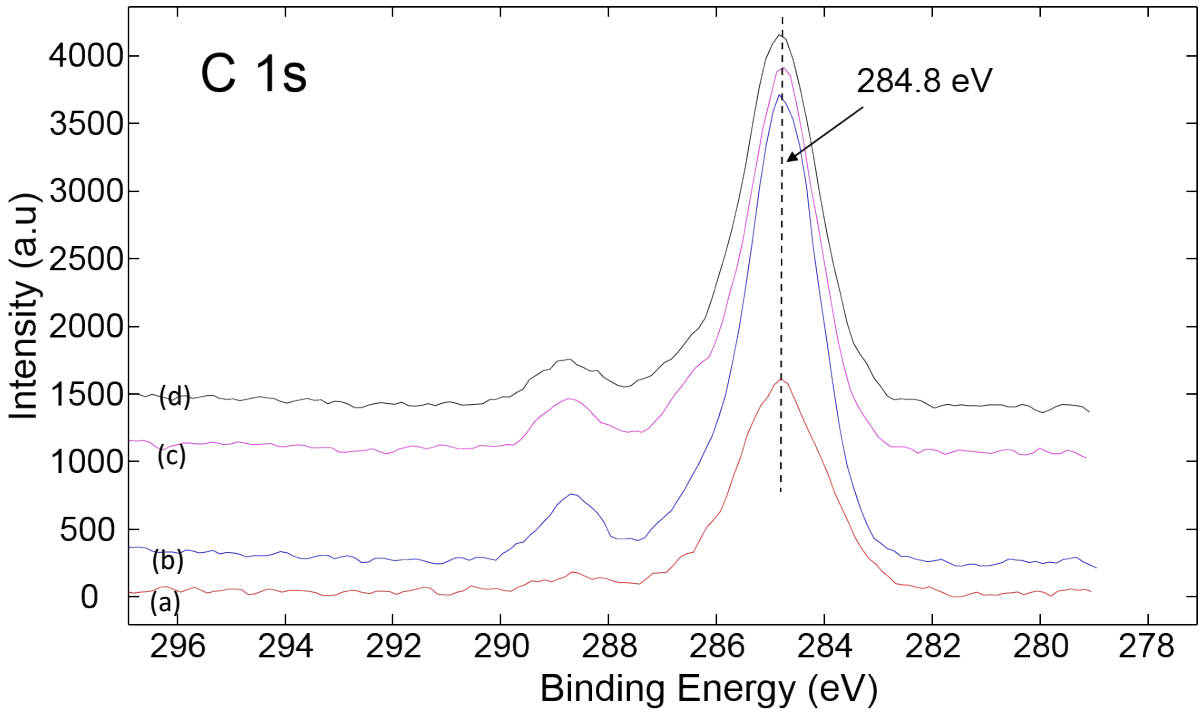

Figure S12 : XPS high energy resolution spectra C 1s from (a) pure sample, (b) reduced sample, (c) sample oxidised at 300 °C (with NO) and (d) sample oxidised at 500 °C (with NO).

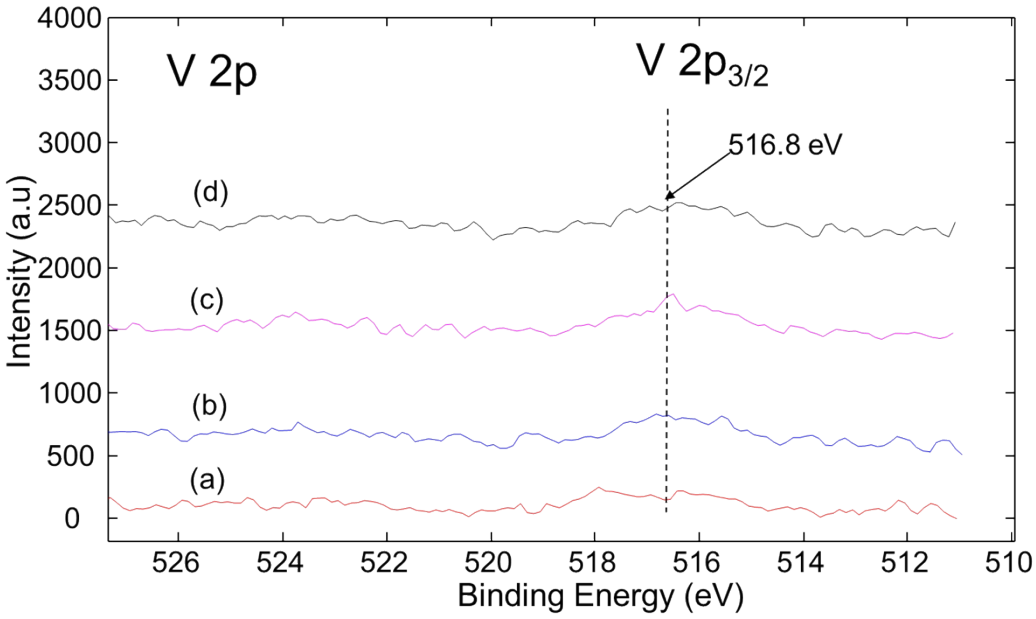

Figure S13 : XPS high energy resolution spectra V 2p from (a) pure sample, (b) reduced sample, (c) sample oxidised at 300 °C (with NO) and (d) sample oxidised at 500 °C (with NO).

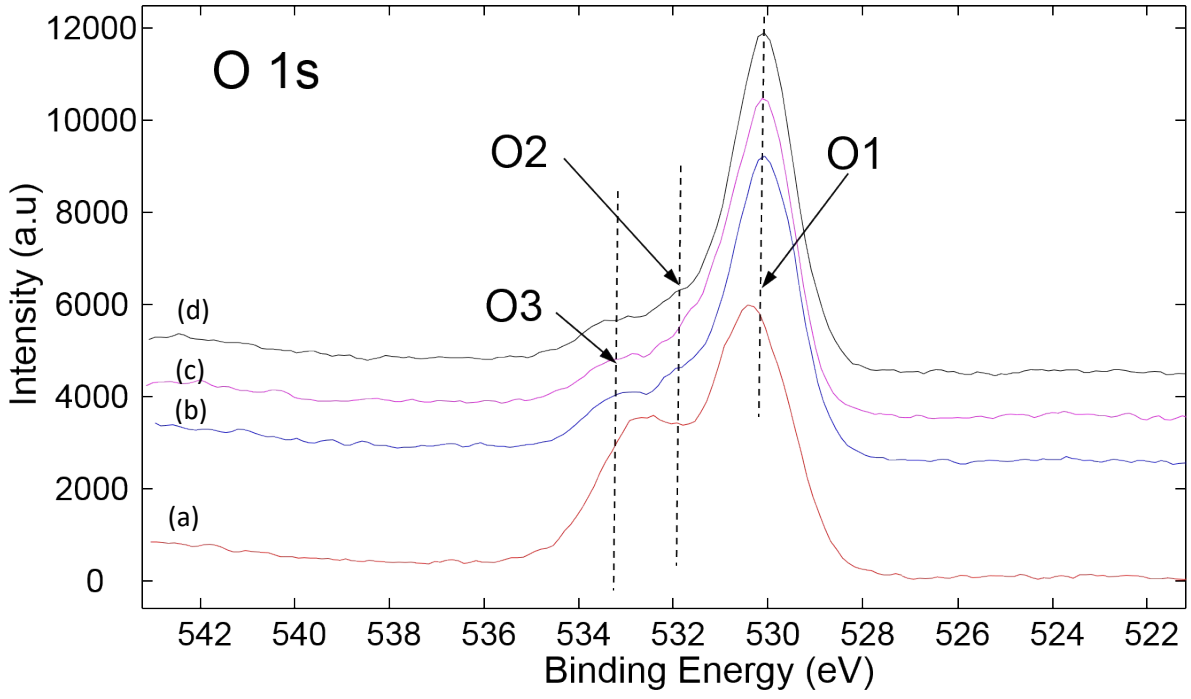

Figure S14 : XPS high energy resolution spectra of O 1s from (a) pure sample, (b) reduced sample, (c) sample oxidised at 300 °C (with NO) and (d) sample oxidised at 500 °C (with NO).

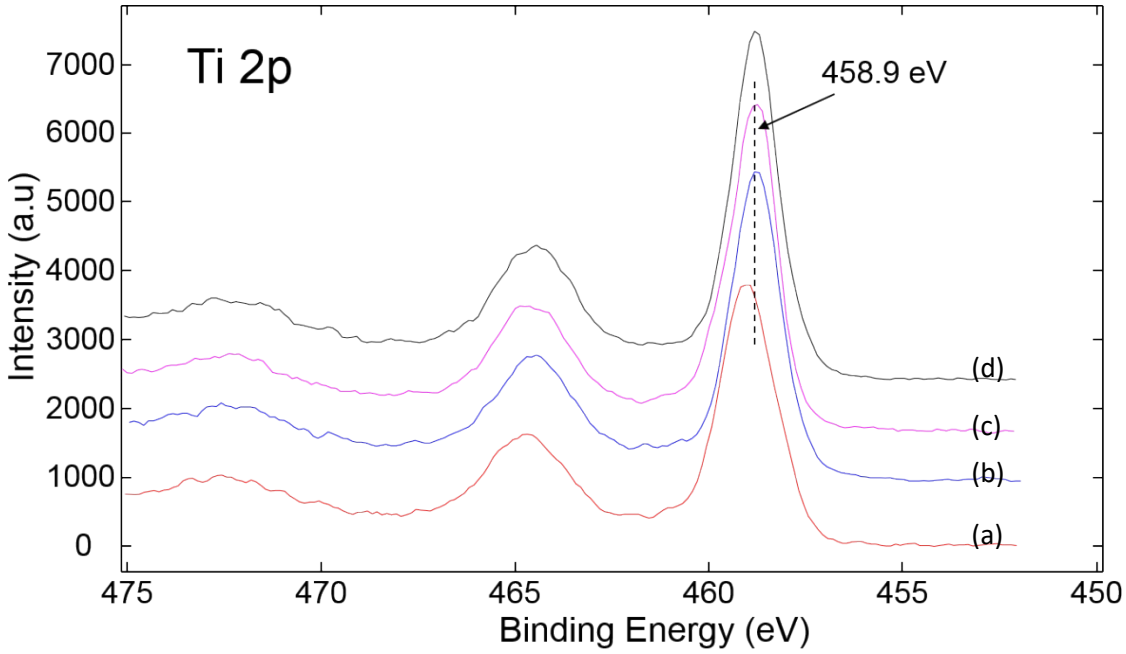

Figure S15 : XPS high energy resolution spectra of Ti 2p from (a) pure sample, (b) reduced sample, (c) sample oxidised at 300 °C (with NO) and (d) sample oxidised at 500 °C (with NO).

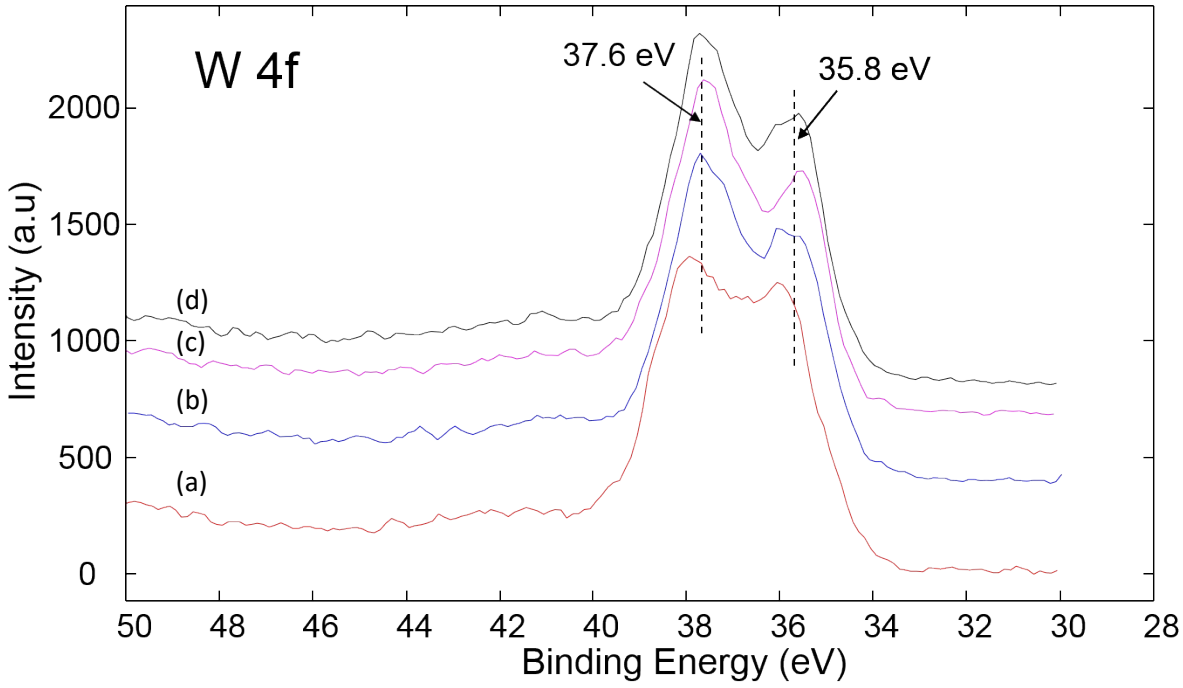

Figure S16 : XPS high energy resolution spectra of W4f from (a) pure sample, (b) reduced sample, (c) sample oxidised at 300 °C (with NO) and (d) sample oxidised at 500 °C (with NO). Peak corresponding to W 4f overlap with Ti 3s peak at 37.6 eV.

Table S6: Surface chemical composition obtained from XPS data of the catalysts treated at different conditions

Condition	C (at.%)	O (at.%)	Si (at.%)	Ti (at.%)	V (at.%)	W (at.%)
Fresh	30.5	49.2	7.4	9.4	0.7	2.9
Reduced	43.4	41.5	1.3	10.6	0.6	2.7
Oxidised at 300 ºC (with NO)	38.3	44.2	1.3	12.2	1.1	3.0
Oxidised at 500 ºC (with NO)	42.1	41.7	2.4	10.6	0.3	2.8

Table S7: Concentration of various oxygen species obtained from XPS data of the catalysts treated at different conditions

Condition	O1 (%)	O2 (%)	O3 (%)
Fresh	59	17	24
Reduced	73	16	11
Oxidised at 300 ºC (with NO)	73	17	10
Oxidised at 500 ºC (with NO)	78	12	10

References

[1] V.D.B.C. Dasireddy, M. Hus, B. Likozar, Effect of O2, CO2 and N2O on Ni-Mo/Al2O3 catalyst oxygen mobility in n-butane activation and conversion to 1,3-butadiene, Catal. Sci. Tech., 7 (2017) 3291-3302.
[2] T. Degen, M. Sadki, E. Bron, U. König, G. Nénert, The HighScore suite, Powder Diffraction, 29 (2014) S13-S18.
[3] A. Coelho, TOPAS Academic Version 4.1 Technical Reference, Coelho Software, 2007.
[4] I.E. Wachs, J.-M. Jehng, G. Deo, B.M. Weckhuysen, V.V. Guliants, J.B. Benziger, S. Sundaresan, Fundamental Studies of Butane Oxidation over Model-Supported Vanadium Oxide Catalysts: Molecular Structure-Reactivity Relationships, J. Catal., 170 (1997) 75-88.
[5] I.E. Wachs, J.-M. Jehng, G. Deo, B.M. Weckhuysen, V.V. Guliants, J.B. Benziger, In situ Raman spectroscopy studies of bulk and surface metal oxide phases during oxidation reactions, Catal. Today, 32 (1996) 47-55.
[6] J.C. Jung, H. Kim, A.S. Choi, Y.-M. Chung, T.J. Kim, S.J. Lee, S.-H. Oh, I.K. Song, Effect of pH in the preparation of γ-Bi2MoO6 for oxidative dehydrogenation of n-butene to 1,3-butadiene: Correlation between catalytic performance and oxygen mobility of γ-Bi2MoO6, Catal. Commun., 8 (2007) 625-628.
[7] R. Grasselli, Fundamental Principles of Selective Heterogeneous Oxidation Catalysis, Top. Catal., 21 (2002) 79-88.
[8] J.-H. Park, C.-H. Shin, Oxidative dehydrogenation of butenes to butadiene over Bi–Fe–Me(Me = Ni, Co, Zn, Mn and Cu)–Mo oxide catalysts, J Ind. Eng. Chem., 21 (2015) 683-688.
[9] J.A. Toledo, P. Bosch, M.A. Valenzuela, A. Montoya, N. Nava, Oxidative dehydrogenation of 1-butene over Zn□Al ferrites, J. Mol. Catal. A: Chem., 125 (1997) 53-62.
[10] Y.-M. Chung, Y.-T. Kwon, T.J. Kim, S.J. Lee, S.-H. Oh, Prevention of Catalyst Deactivation in the Oxidative Dehydrogenation of n-Butene to 1,3-Butadiene over Zn-Ferrite Catalysts, Catal. Lett., 131 (2009) 579-586.
[11] I.-C. Marcu, I. Sandulescu, J.-M.M. Millet, Oxidehydrogenation of n-butane over tetravalent metal phosphates based catalysts, Appl. Catal., A, 227 (2002) 309-320.
[12] B.R. Jermy, B.P. Ajayi, B.A. Abussaud, S. Asaoka, S. Al-Khattaf, Oxidative dehydrogenation of n-butane to butadiene over Bi–Ni–O/γ-alumina catalyst, J. Mol. Catal. A: Chem., 400 (2015) 121-131.
[13] A. Gervasini, Temperature Programmed Reduction/Oxidation (TPR/TPO) Methods, in: A. Auroux (Ed.) Calorimetry and Thermal Methods in Catalysis, Springer Berlin Heidelberg, Berlin, Heidelberg, 2013, pp. 175-195.